Generalization of coupled spiking models and effects of the width of an action potential on synchronization phenomena

Yasuomi Daishin Sato[1,2,*] and Masatoshi Shiino[2]
[1]*Frankfurt Institute for Advanced Studies, Johann Wolfgang Goethe University, Max-von-Laue-Str. 1, D-60438 Frankfurt am Main, Germany*
[2]*Department of Physics, Faculty of Science, Tokyo Institute of Technology, 2-12-1 Oh-okayama, Meguro-ku, Tokyo 152-0033, Japan*
(Received 8 February 2006; revised manuscript received 23 July 2006; published 11 January 2007)

The integrate-and-fire (IF) neuron model and the piecewise-linear version of FitzHugh-Nagumo (PL) neuron model with a time scale parameter μ are frequently being used in the study of synchronization phenomena. Although the two models are regarded to be different type, we show a certain equivalence between them by deriving the coupled IF model of an improved version with a firing duration from the recovery variable coupled system of the PL model, under taking the limit of $\mu \to 0$ without a loss of any coupling properties. In the coupled IF model with the duration time, the synchronization behavior of a pair of neurons with excitatory or inhibitory synaptic coupling can be systematically explored in terms of three parameters in the model (synaptic strength, decaying relaxation rate of the synaptic coupling, and the parameter exhibiting the firing duration). We find some irregularly synchronous behavior with or without constant firing order alternations. We show that the duration of an impulse plays an important role in synchronization phenomena.

DOI: 10.1103/PhysRevE.75.011909 PACS number(s): 87.10.+e, 02.60.Cb, 05.45.Xt

I. INTRODUCTION

Mammalian nervous systems exhibit a diversity of synchronized behaviors such as a transition from a periodic orbit to a chaotic attractor, attraction to a periodic orbit, and noise-induced synchronization [1–4]. It has been supposed that theoretical studies of such synchronized behaviors in neuronal assemblies play an important role in our understanding of information processing in the nervous systems.

A prominent example in which the nonlinear dynamic behavior has been successfully studied is the synchronous firing of interconnected neurons. Such synchronous firing can be found in the sensory processing of cat visual cortex [5–7]. Synchronized behavior in the nervous systems can be frequently illustrated as a nonlinear dynamical model of large and small numbers of coupled oscillators [8–15].

There have thus far been many models for the synaptic interactions between neurons. As a representative of the standard synaptic model, two types of coupling are found in a real nervous system. One is the chemical synapse while the other is the electrical synapse [12,13]. In particular, the electrical synapse has been regarded as a plausible mechanism for controlling synchronized oscillations in inhibitorily coupled neurons [16,17].

Regarding the intrinsic membrane properties, various types of neuronal oscillators, ranging from theoretically tractable models to biophysical conductance-based models [18–21], have been put forward. In particular, for the theoretically tractable model, integrate-and-fire (IF) [22], FitzHugh-Nagumo (FHN) [23,24], and piecewise-linear (PL) models [25] are well known as mathematical models of neural activity. They can frequently be classified into types I and II due to the different dynamical properties. If in the type I model, a constant applied current is slowly increased, the neuronal dynamic changes from stationary to oscillatory with zero frequency. Meanwhile for the type II model, the onset occurs with nonzero frequency. The IF model is regarded as type I while the FHN and PL models are type II [26–28].

In general, the FHN model is given by

$$\frac{dx}{dt} = -\frac{1}{3}x^3 + x - y + I_{app}, \tag{1}$$

$$\frac{dy}{dt} = \mu(x + a - by), \tag{2}$$

where x is called the excitation variable and represents the membrane potential, while y is called the recovery variable [29], a and b are constants. I_{app} is the applied current and $\mu(>0)$ is a time scale parameter.

This model has sometimes been utilized in order to find noise-induced synchronization in real neurons and electrical circuits [3,30]. The specific position of a noise source in the FHN model [that is dependent on whether the noise source is in Eq. (1) or Eq. (2)] was thought to be very important for quantitative estimations. The effect of noise in Eq. (2) appears to be much more dominant compared to inserting into Eq. (1), [3]. However, a comparison of whether the coupling term taking the same form is inserted into the x or y dynamics has not yet been performed.

The IF model has high practicality for modeling behavior in real nervous systems, in spite of very simple firing dynamics without the firing duration [11,31,32]. Improved versions of the IF models with a refractory period [33,34] or a firing duration have also been suggested. One can also see the IF model exhibiting exponentially rapid rising membrane potential after having fired [35] and the double integrate-and-fire (DIF) model [36,37]. The study using the former model shed light on the fact that shape and size of the neuron spike play a role in the scheme of synchronization phenomena in either two or more electrically coupled neurons.

It has been widely known that the FHN model as above is a simplification of the biophysical conductance-based model

*Electronic address: sato@fias.uni-frankfurt.de

such as the Hodgkin-Huxley (HH) model. But it is still unclear how the standard as well as improved IF models are simplified from another theoretically tractable or biophysical conductance-based model. No one has discussed whether the above classification between the IF and PL (or FHN) models can be validated.

The aim of this paper is to study the qualitative relationship between systems of a pair of coupled IF neurons and the coupled PL ones. For this aim, we are interested in synchronous behavior of the coupled PL neurons for the case that the synaptic coupling is added in the y dynamics of the PL models. We analyze an accurately solvable model of two neurons coupled via chemical synapses. We find out how the width of an action potential of neuron models, as well as dynamic properties of synaptic coupling, influences a scheme of synchronized oscillations.

The outline of this paper is as follows. In Sec. II, we use two interconnected neural oscillators of the PL type with excitatory or inhibitory synaptic couplings. The phase plane analysis using the singular perturbation approach [38–41] is employed, because the PL model in general demonstrates relaxation oscillations that split the dynamics into slow and fast components. For synaptic coupling, we use first-order kinetics of the gating variable for inactivation [42] instead of incorporating an α function [43]. Moreover, we introduce an assumption that dynamics for recovery and synaptic variables, which can be parametrized by the same time scale, are slower than membrane potential dynamics. We investigate the difference between cases in which the synaptic coupling is in the membrane potential or the recovery dynamics. By using these ideas, we show that as $\mu \to 0$, the membrane potential oscillates between the active and inactive phases with instantaneous transitions between the two phases [44–47]. Interestingly enough, the y-coupled PL model is generalized to the coupled IF one without a loss of dynamic properties in the synaptic models.

In Sec. III, we make use of a return map of the solutions to the y-coupled PL equations, in order to investigate the role of the width of an action potential in synchronization phenomena. The return map can be analytically constructed by assigning the iterated point as the state of two coupled neurons that occur immediately after one of them has fired. Such a map enables us to investigate the condition in which the two-neuron system achieves a completely synchronous state (often called in-phase synchronization) as well as the out-of-phase state (for example, the antiphase synchronization), in terms of the parameters of the synaptic model and the neuron model.

In Sec. IV, we present the results by drawing a phase diagram of the parameter space of the strength and the decaying relaxation rate of synaptic couplings, due to the differing width of an action potential. In the case of excitatory coupling, if the decaying relaxation rate is large, two neurons approach the synchronous state, but not a complete synchronous state. When the rate is small, they show an antiphase state. They go forward in-phase or quasi-in-phase for any decaying rates, depending on the firing duration. In the case of inhibitory coupling, differences between the two neurons change from in phase or antiphase states to only the in-phase state, depending on the initial conditions and the decaying relaxation rate of the synaptic coupling. In particular, when strong coupling occurs, various irregular synchronization phenomena are found. These results are in agreement with numerical simulations, which are conducted using the fourth-order Runge-Kutta method for the FHN and the PL models. In order to survey a region of a time scale parameter μ where the return map method can be applied, we employ a phase reduction method [48–52]. The phase reduction method has been a well-known and useful analysis of synchronous behavior in nonlinear dynamical systems exhibiting oscillations. When neuron models of the PL or FHN types are mutually connected by weak couplings, the coupled systems can be reduced to a system consisting of the phase degrees of freedom. We give a discussion and conclusion in Secs. V and VI.

II. GENERALIZATION OF SPIKING NEURONS WITH SYNAPTIC COUPLING

We shall begin by introducing a different assumption of two interconnected neural oscillators of the PL type with excitatory or inhibitory synaptic coupling. We assume that the time scale ($\mu > 0$) for the y variable is the same as the one for synaptic responses. Therefore we write this coupled model in the general form:

$$\frac{d\mathbf{X}_i}{dt} = F_i(\mathbf{X}_i) + G_i(\mathbf{X}_{\bar{i}}) \quad (i = 1,2), \tag{3}$$

where $\bar{i}$ represents a counterpart of the ith neuron. $\bar{i}=2$ if $i=1$ and vice versa. $\mathbf{X}_i=(x_i,y_i,s_i)^T \in \mathbb{R}^3$ and ^{T} denotes transpose. x_i is a fast variable while y_i and s_i are slow recovery and synaptic variables, respectively. While $G_i(\mathbf{X}_{\bar{i}})$ represents a coupling vector, $F_i(\mathbf{X}_i)$ is a baseline vector field:

$$F_i(\mathbf{X}_i) = \begin{pmatrix} f(x_i,y_i) \\ \mu g(x_i,y_i) \\ \mu h(x_i,s_i) \end{pmatrix}, \tag{4}$$

$$f(x_i,y_i) = F_{\mathrm{PL}}(x_i) - y_i + I_{app}, \tag{5}$$

$$g(x_i,y_i) = x_i + a - by_i, \tag{6}$$

$$h(x_i,s_i) = \begin{cases} 0 \to s_i = 1 & (x_i \geqslant \theta_1), \\ -\beta s_i & (x_i < \theta_1), \end{cases} \tag{7}$$

where

$$F_{\mathrm{PL}}(x) = \begin{cases} -mx + (p+m)\theta_1 + q, & \text{for } x \leqslant \theta_1, \\ px + q, & \text{for } \theta_1 < x < \theta_2, \\ -nx + (p+n)\theta_2 + q, & \text{for } \theta_2 \leqslant x. \end{cases} \tag{8}$$

$p(>0)$, q, $m(>0)$, and $n(>0)$ are constants. θ_1 and θ_2 are x values respectively at the left and right knee of x-nullcline as shown in Fig. 1(a). We suppose that $\theta_1 < [a+b(I_{app}-q)]/(bp-1) < \theta_2$ and $p < 1/b$ so that the model represents an oscillatory system exhibiting spontaneous periodic firing. In particular, $p=2/3$, $q=0$, $m=n=4/3$, $\theta_1=-1$, $\theta_2=1$, and

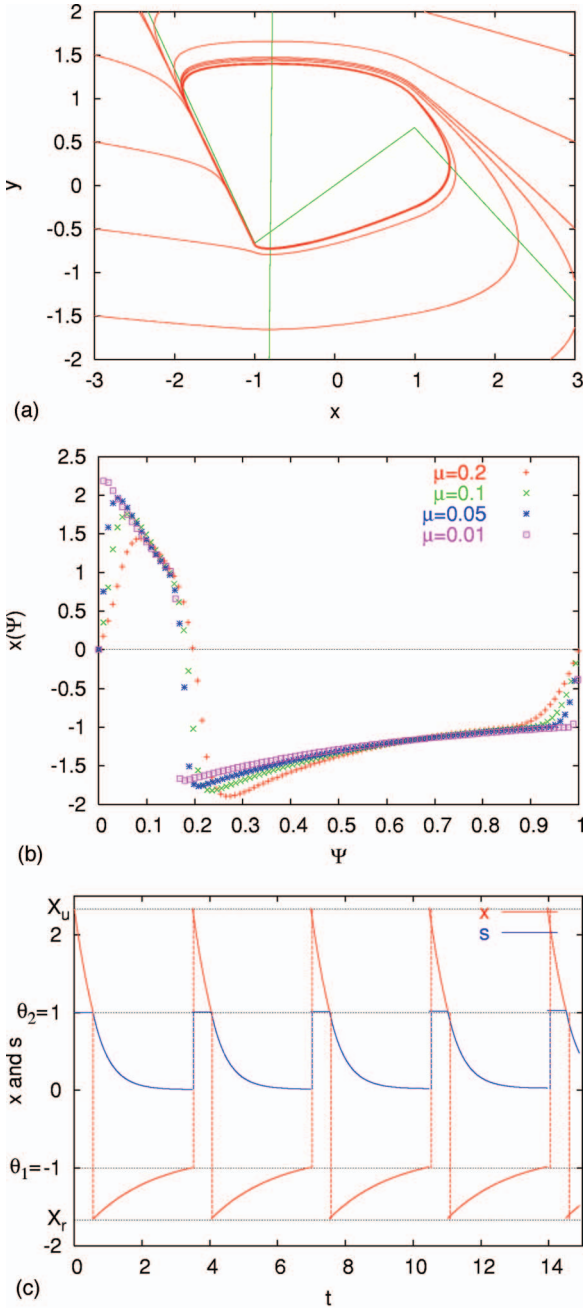

FIG. 1. (Color) Singular perturbation approach of the PL model. (a) Phase plane of the PL model with $\mu=0.2$. The red lines indicate dynamical flow while the green lines present the nullclines, those are $\dot{x}=0$ and $\dot{y}=0$. (b) Time evolutions of membrane potential x as μ becomes smaller. The temporal duration between points means a velocity of x. The x motion on the active or inactive phases becomes gradually slower. Ψ is a variable normalized by a periodicity. (c) $\mu\to 0$; membrane potential and synaptic response are represented, respectively, as the red and blue lines. Here we set $a=0.8$, $b=0.01$, $p=2/3$, $q=0$, $m=2$, $n=1$, $\theta_1=-1$, $\theta_2=1$, and $\beta=1$.

$I_{app}=0$ enable us to show the PL type of the FHN model [46]. The phase plane (x,y) can be appropriately used as a geometrical tool. The x nullcline (defined by $dx/dt=0$) has an inverted N-shape while the y nullcline is monotonically increasing. Both the nullclines are represented as green lines in Fig. 1(a). In previous studies, y has been often regarded as a gating variable of a total ionic channel in the HH model by piecewise linearization as a geometrical tool in the phase plane [57,58]. However, in this study, it would represent the membrane potential but not such a gating variable, because the singular perturbation approach with μ allows us to obtain a linear equation of x and y [as described in detail below, Eq. (14)].

For Eq. (7), we incorporate a first-order kinetics instead of an α function. β is the synaptic decaying relaxation rate, as shown in Fig. 1(c). The synapse response can be generally regarded to be slowly varying [53]. In real neurons, it has been experimentally observed that such responses are slower than the time scale for the action potential [54–56]. For the coupling vector $G_i(\mathbf{X}_i^-)$, we select two kinds of vectors,

$$(0,-\mu g_{syn} s_i^-,0)^T \tag{9}$$

and

$$(g_{syn} s_i^-,0,0)^T, \tag{10}$$

where g_{syn} shows the synaptic strength. For Eq. (9), it represents respectively excitatory and inhibitory couplings for $0<g_{syn}<\{[(\theta_2-a)/b]-p\theta_2-q-I_{app}\}b$ and $\{[(\theta_1+a)/b]-p\theta_1-q-I_{app}\}b<g_{syn}<0$. Meanwhile, for Eq. (10), excitatory and inhibitory couplings are shown when $0<g_{syn}<[(\theta_2-a)/b]-p\theta_2-q-I_{app}$ and $[(\theta_1+a)/b]-p\theta_1-q-I_{app}<g_{syn}<0$. We notice that cases using another coupling such as diffusive coupling, α functions with or without a reversal potential, are also satisfied by the following approach.

We consider the case of $G(\mathbf{X}_i^-)=(0,-\mu g_{syn} s_i^-,0)^T$. To switch from fast dynamics to slow, we change the time scale to $\tau=\mu t$ and rewrite the coupled PL equation:

$$\mu\frac{dx_i}{d\tau}=F_{\mathrm{PL}}(x_i)-y_i+I_{app}, \tag{11}$$

$$\frac{dy_i}{d\tau}=x_i+a-by_i-g_{syn}s_i^-, \tag{12}$$

$$\frac{ds_i}{d\tau}=h(x_i,s_i). \tag{13}$$

As μ becomes smaller, the motions in the active and silent phases become slower while the switching motions between them become faster [Fig. 1(b)]. Then, taking the limit $\mu\to 0$, a simplified PL model is obtained:

$$0=F_{\mathrm{PL}}(x_i)-y_i+I_{app}, \tag{14}$$

$$\frac{dy_i}{d\tau}=x_i+a-by_i-g_{syn}s_i^-, \tag{15}$$

$$\frac{ds_i}{d\tau}=h(x_i,s_i). \tag{16}$$

Here the transition between the silent and active phases becomes instantaneous because $dy/dt=0$ as the time scale is not changed and $\mu\to 0$. These equations are the simplified

version of the coupled PL model. They ignore the switching motions between the active and inactive phases and give attention only to the active and inactive phases. We depict Fig. 1(c) to show that the trajectory follows a vertical broken line to enter the active or inactive phases after arriving at θ_1 or θ_2. It is illustrated as the firing dynamic that occurs when x arrives at θ_1 and instantaneously jumps up to $X_u(=[p(\theta_2-\theta_1)+n\theta_2+I_{app}]/n)$. Then, it exponentially decays to θ_2, after which it is abruptly reset to $X_r(=[p(\theta_1-\theta_2)+m\theta_1+I_{app}]/m)$.

We continue by differentiating Eq. (14) with respect to τ. Thus we obtain

$$\frac{dy_i}{d\tau} = -\frac{\partial F_{\mathrm{PL}}(x_i)}{\partial x}\frac{dx_i}{d\tau}. \tag{17}$$

Using Eqs. (14) and (17), Eq. (15) is transformed to a one-dimensional differential model for the x variable with a coupling, which is given by

$$\frac{dx_i}{d\tau} = F_{\mathrm{DIF}}(x_i) + G_{syn}s_i^-, \tag{18}$$

$$\frac{ds_i}{d\tau} = h(x_i, s_i), \tag{19}$$

$$F_{\mathrm{DIF}}(x) = \begin{cases} -\gamma_1 x + X_1, & \text{for } x \in [\theta_2, \infty], \\ -\gamma_0 x + X_0, & \text{for } x \in [-\infty, \theta_1], \end{cases} \tag{20}$$

where $G_{syn}=g_{syn}/k, k=m$ (for $x \geqslant \theta_1$) or n (for $x \geqslant \theta_2$). $\gamma_0 = b+1/m$, $\gamma_1 = b+1/n$, $X_0=\{-a+b[(p+m)\theta_1+q+I_{app}]\}/m$ and $X_1=\{-a+b[(p+n)\theta_2+q+I_{app}]\}/n$. It is noted that the transition $\mu \to 0$ would leave the structure of the phase space intact. Equation (20) is called the double integrate-and-fire (DIF) model.

We can easily expect that γ_1 determines the firing duration. As $\gamma_1 \to \infty$, the width of action potential vanishes. As a result, we find that a simplified version of the coupled PL model becomes precisely equal to the coupled original IF model:

$$\frac{dx_i}{dt} = X_0 - \gamma_0 x_i + G_{syn}s_i^-, \tag{21}$$

where the regime of x is only in $[-\infty, \theta_1]$. As soon as the activation variable x arrives at the threshold $(x=\theta_1)$ (because the neuron is regarded as already having fired), it is reset to X_r.

The case of $G(\mathbf{X}_i^-, t)=(g_{syn}s_i^-, 0, 0)^T$ has already been pursued in previous studies [37,39,44]. Treating this case with a similar approach as mentioned above, the simplified PL model is obtained as follows:

$$0 = F_{\mathrm{PL}}(x_i) - y_i + I_{app} + g_{syn}s_i^-, \tag{22}$$

$$\frac{dy_i}{d\tau} = x_i + a - by_i, \tag{23}$$

$$\frac{ds_i}{d\tau} = h(x_i, s_i). \tag{24}$$

This indicates that in the phase plane analysis, the x_i nullcline was shifted upward by receiving an excitatory synaptic input from neuron $\bar{i}$. If the state of neuron i is below the local minima of the upward-shifted x_i nullcline, it is forced to enter the active phase of the new nullcline. Then, by using Eq. (22) and its conversion,

$$\frac{dy_i}{d\tau} - g_{syn}\frac{ds_{\bar{i}}^-}{d\tau} = -\frac{\partial F_{\mathrm{PL}}(x_i)}{\partial x}\frac{dx_i}{d\tau}, \tag{25}$$

Eq. (23) is then rewritten as

$$\frac{dx_i}{d\tau} = F_{\mathrm{DIF}}(x_i) + G_{syn}\left(bs_{\bar{i}}^- + \frac{ds_{\bar{i}}^-}{d\tau}\right), \tag{26}$$

$$\frac{ds_i}{d\tau} = h(x_i, s_i). \tag{27}$$

As a result, even though $\gamma_1 \to \infty$, we find the IF model with the transformed synaptic coupling:

$$\frac{dx_i}{dt} = X_0 - \gamma_0 x_i + G_{syn}\left(bs_{\bar{i}}^- + \frac{ds_{\bar{i}}^-}{d\tau}\right). \tag{28}$$

We have revealed a qualitatively consistent relation between the PL and the IF models with synaptic coupling when the synaptic interaction term is inserted into the y dynamics of the PL model.

In conclusion, the resulting different interaction terms of Eqs. (21) and (28) lead to deeper understanding of the dynamical behavior of the coupled PL models, because the behavior undoubtedly depends on whether the coupling term is inserted into x or y dynamics. In fact, such a difference between two types of the insertions is also observed in constructing return maps to investigate synchronous behavior. This will be explained below.

III. ANALYSIS FOR STATES OF THE TWO COUPLED NEURONS

In order to clarify the detailed difference between additions of coupling term to x and y dynamics of the PL model, we need to systematically understand the behavior of the dynamics of the two coupled neurons. To this end, it is very convenient to analytically construct a return map corresponding to the time evolution of Eqs. (18)–(20) or (26) and (27) [the system of Eqs. (26) and (27) is referred to [46]]. The return map analysis is regarded to be a good approach for observations of the system into mathematically rigorous map for the spike times between neurons [59]. Actually, it enables us to gain some solutions exhibiting synchronization phenomena in the two neurons with excitatory or inhibitory synaptic couplings, according to the properties of neural or synaptic dynamics.

A. Construction of return map

We proceed to solve Eqs. (18)–(20) by taking into account three fundamental cases.

TABLE I. Type-I time evolution of neurons 1 and 2 (type-I temporal firing pattern diagram). The number of cases is 3. "+" and "−" indicate that each neuron is firing and not firing.

Duration	Case	Neuron 1	Neuron 2
$[0,\Delta_1]$	1	+	+
$[\Delta_1,\Delta_1+\Delta_2]$	2	+	−
$[\Delta_1+\Delta_2,\Delta_1+\Delta_2+\Delta_3]$	3	−	−
$[\Delta_1+\Delta_2+\Delta_3,\Delta_1+\Delta_2+\Delta_3+\Delta_4]$	2	−	+

Case (i). Both neurons $(i=j)$ are firing,

$$x_i^{++}(t) = x_i^{++}(t_0)e^{-\gamma_1(t-t_0)} + A_1\{1 - e^{-\gamma_1(t-t_0)}\}, \tag{29}$$

$$s_i^{+}(t) = 1. \tag{30}$$

Case (ii). One neuron (i) is firing while the other (j) is not $(i,\ j=1,2)$,

$$x_i^{+-}(t) = x_i^{+-}(t_0)e^{-\gamma_1(t-t_0)} + A_2\{1 - e^{-\gamma_1(t-t_0)}\} + B_1 s_j^{-}(t_0)\{e^{-\beta(t-t_0)} - e^{-\gamma_1(t-t_0)}\}, \tag{31}$$

$$s_i^{+}(t) = 1, \tag{32}$$

$$x_j^{-+}(t) = x_j^{-+}(t_0)e^{-\gamma_0(t-t_0)} + A_3\{1 - e^{-\gamma_0(t-t_0)}\}, \tag{33}$$

$$s_j^{-}(t) = s_j^{-}(t_0)e^{-\beta(t-t_0)}. \tag{34}$$

Case (iii). Neither neuron $(i=j)$ is firing,

$$x_i^{--}(t) = x_i^{--}(t_0)e^{-\gamma_0(t-t_0)} + A_4\{1 - e^{-\gamma_0(t-t_0)}\} + B_2 s_j^{-}(t_0)\{e^{-\beta(t-t_0)} - e^{-\gamma_0(t-t_0)}\}, \tag{35}$$

$$s_i^{-}(t) = s_i^{-}(t_0)e^{-\beta(t-t_0)}, \tag{36}$$

where $A_1=[X_1+G_{syn}]/\gamma_1$, $A_2=X_1/\gamma_1$, $A_3=[X_0+G_{syn}]/\gamma_0$, $A_4=X_0/\gamma_0$, $B_1=G_{syn}/[\gamma_1-\beta]$, and $B_2=G_{syn}/[\gamma_0-\beta]$ and the left symbol in the superscripts of x_i means that neuron i is firing or not while its right represents the state of a counterpart of i. Although we have investigated the solutions in the case of $\beta\neq\gamma_0$ and γ_1, the following analyses would be solved even in the cases of $\beta=\gamma_0$ and γ_1 as well as $\gamma_1\to\infty$.

Next, we focus on the state of the two neurons that exists immediately after one of the neurons has fired. Supposing that $t=0$ immediately after the membrane potential of neuron 1 has crossed the threshold θ_1; let $x_1^{++}(0)$ [or $x_1^{+-}(0)$]$=x_1^{(n)}\equiv X_u$, $x_2^{++}(0)$ [or $x_2^{-+}(0)$]$=x_2^{(n)}$, $s_1^{+}(0)=s_1^{(n)}$, and $s_2^{+}(0)$ [or $s_2^{-}(0)$]$=s_2^{(n)}$ denote the values of x_i and s_i $(i=1$ and $2)$ for the nth occurrence of such states.

With the use of the three fundamental cases above, the so-called temporal firing pattern diagrams (TFPDs) are obtained. They represent how each neuronal firing dynamic transits from the active phase to the inactive phase and vice versa. The simplest and most important TFPDs are shown in Tables I and II.

Table I shows that, supposing both the neurons are firing, one neuron that stops firing earlier can start firing again to become active after the other neuron stops firing. Here we notice appearances of difference of y coupling and x coupling in constructions of the TFPD. This can be geometrically explained by using the phase plane in Sec. II.

TABLE II. Type-II time evolution of neurons 1 and 2 (type-II temporal firing pattern diagram).

Duration	Case	Neuron 1	Neuron 2
$[0,\Delta_1]$	2	+	−
$[\Delta_1,\Delta_1+\Delta_2]$	3	−	−
$[\Delta_1+\Delta_2,\Delta_1+\Delta_2+\Delta_3]$	2	−	+
$[\Delta_1+\Delta_2+\Delta_3,\Delta_1+\Delta_2+\Delta_3+\Delta_4]$	3	−	−

For Eqs. (18)–(20), in the x-y plane, a nullcline of $dy/dt=0$ can be shifted in the phase plane through the effect of the coupling term. The shift means that as neuron 1, for example, receives an excitatory stimulus from neuron 2, the state of neuron 1 is forced to be on the left branch of x nullcline until its local minima $(\theta_1, p\theta_1+q)$, in order to enter the right branch. However, for Eqs. (22)–(24) [or Eqs. (26) and (27)], the x nullcline of neuron 1 is shifted upward by receiving an excitatory synaptic stimulus from neuron 2. Then, the state of neuron 1 can come below $(\theta_1, p\theta_1+q+I_{syn})$ to start entering the right branch of the new nullcline. This is a crucial mechanism that both the neurons can simultaneously fire in the x-coupling dynamic. The details are referred to [46]. Therefore we do not need a final temporal diagram, $[\Delta_1+\Delta_2+\Delta_3,\Delta_1+\Delta_2+\Delta_3+\Delta_4]$ of the type-I TFPD.

Table II demonstrates that, supposing both the neurons are inactive, one neuron that starts to fire earlier can stop firing to become inactive before the other neuron starts to fire.

In accordance with such features of TFPDs, one- or two-dimensional return maps are then constructed as

$$x_2^{(n)} \mapsto x_2^{(n+1)} \tag{37}$$

or

$$\begin{pmatrix} x_2^{(n)} \\ s_2^{(n)} \end{pmatrix} \mapsto \begin{pmatrix} x_2^{(n+1)} \\ s_2^{(n+1)} \end{pmatrix} \tag{38}$$

together with defining some synchronized solution, which is represented as the time-lag rate between firings of the two neurons at the nth iterate: $\phi(x_2^{(n)})$ [or $\phi(x_2^{(n)}, s_2^{(n)})$]$\equiv T'/T$. Here T represents neuron 1's spike interval while T' shows the duration that it takes for neuron 2 to start firing after neuron 1 has already fired. The solutions are also given by $\phi=1$ (or 0): the in-phase synchronized solution, $0.75\leqslant\phi<1$ (or $0<\phi\leqslant 0.25$): the quasi-in-phase synchronized solution, $0.5<\phi<0.75$ (or $0.25<\phi<0.5$): the quasi-antiphase synchronized solution, and $\phi=0.5$: the antiphase synchronized solution. The in phase (or the antiphase) synchronized solution is very similar to the quasi-in-phase (or the quasi-antiphase) synchronized solution. However, such a classification would be needed in order to find the effect of the firing duration on synchronization phenomena in a pair of coupled neurons, as described in the following sections.

B. In-phase synchronization

We shall start by finding an effective condition that type-I TFPD can be completely applied to study the one-dimensional return map for the typical analysis of in-phase synchronization behavior without alternating the two neurons' firing order. This condition is specified by the case if one of the two neurons on the inactive phase arrives at the threshold (θ_1) earlier than the other neuron. The condition in which this case occurs can be obtained by considering the temporal diagrams until $\Delta_1+\Delta_2+\Delta_3$ of type-I TFPD. It can also be described in terms of G_{syn} and β as shown in Appendix A. Such (G_{syn}, β) regions [i.e., III–VIII] on the G_{syn}-β plane are illustrated in Fig. 2(a) as an example.

To define the return map corresponding exactly to type-I TFPD where the nth state of the two neurons is set up as $x_1^{(n)} \equiv X_u$, $s_1^{(n)} \equiv 1$, $x_2^{(n)}$, and $s_2^{(n)}=1$, we first suppose that during time interval $[0,\Delta_1]$, neurons 1 and 2 are in the active phase and that at $t=\Delta_1$, neuron 2 stops firing and enters the inactive phase. Using case (i), the state of the two neurons at $t=\Delta_1$ is denoted by

$$x_1^{+-}(\Delta_1) = x_1^{++}(\Delta_1) = x_1^{++}(0)e^{-\gamma_1\Delta_1} + A_1(1-e^{-\gamma_1\Delta_1}), \quad (39)$$

$$s_1^{+}(\Delta_1) = 1, \quad (40)$$

$$x_2^{++}(\Delta_1) = x_2^{++}(0)e^{-\gamma_1\Delta_1} + A_1(1-e^{-\gamma_1\Delta_1}) = \theta_2,$$

$$\rightarrow x_2^{-+}(\Delta_1) = X_r, \quad (41)$$

$$s_2^{+}(\Delta_1) = s_2^{-}(\Delta_1) = 1. \quad (42)$$

Next, let us suppose that for $[\Delta_1,\Delta_1+\Delta_2]$, neuron 2 is in the inactive phase while neuron 1 remains in the active phase. At $t=\Delta_1+\Delta_2$, using case (ii), the state of the two neurons is denoted by

$$x_1^{+-}(\Delta_1+\Delta_2) = x_1^{+-}(\Delta_1)e^{-\gamma_1\Delta_2} + A_2(1-e^{-\gamma_1\Delta_2}) + B_1 s_2^{-}(\Delta_1)(e^{-\beta\Delta_2} - e^{-\gamma_1\Delta_2}) = \theta_2,$$

$$\rightarrow x_1^{--}(\Delta_1+\Delta_2) = X_r, \quad (43)$$

$$s_1^{+}(\Delta_1+\Delta_2) = s_1^{-}(\Delta_1+\Delta_2) = 1, \quad (44)$$

$$x_2^{--}(\Delta_1+\Delta_2) = x_2^{-+}(\Delta_1+\Delta_2) = x_2^{-+}(\Delta_1)e^{-\gamma_0\Delta_2} + A_3(1-e^{-\gamma_0\Delta_2}), \quad (45)$$

$$s_2^{-}(\Delta_1+\Delta_2) = s_2^{-}(\Delta_1)e^{-\beta\Delta_2}. \quad (46)$$

Similarly, suppose that both neurons are in the inactive phase for $[\Delta_1+\Delta_2,\Delta_1+\Delta_2+\Delta_3]$. Using case (iii), the state of the two neurons at $t=\Delta_1+\Delta_2+\Delta_3$ is denoted by

$$x_1^{--}(\Delta_1+\Delta_2+\Delta_3) = x_1^{--}(\Delta_1+\Delta_2)e^{-\gamma_0\Delta_3} + A_4(1-e^{-\gamma_0\Delta_3}) + B_2 s_2^{-}(\Delta_1+\Delta_2)(e^{-\beta\Delta_3} - e^{-\gamma_0\Delta_3}), \quad (47)$$

$$s_1^{-}(\Delta_1+\Delta_2+\Delta_3) = s_1^{-}(\Delta_1+\Delta_2)e^{-\beta\Delta_3}, \quad (48)$$

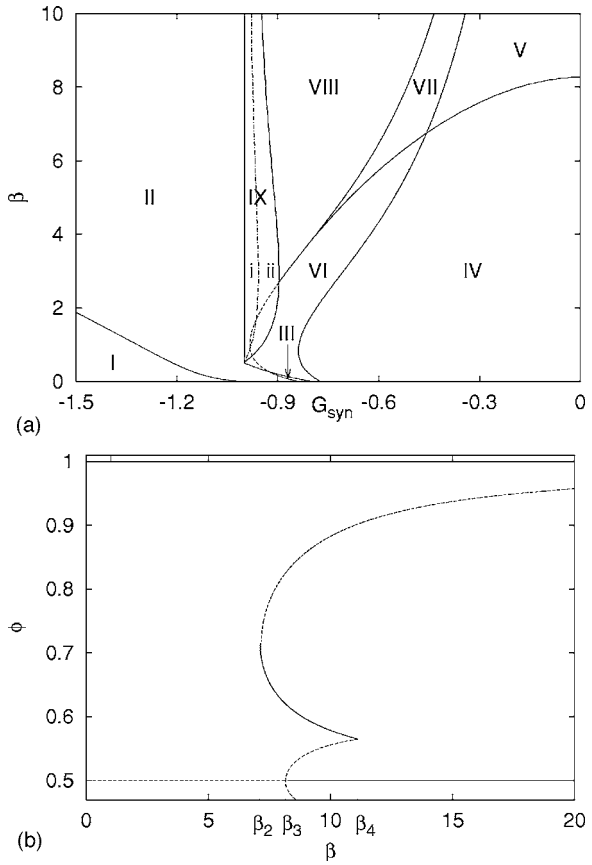

FIG. 2. G_{syn}-β diagram and the bifurcation diagram for a small γ_1 and inhibitory coupling. As $\gamma_1=1.0$ in the case of inhibitory synaptic couplings, (a) G_{syn}-β phase diagram. Region I: death oscillators [as shown in Fig. 3(a)]. Region II: the only antiphase synchronized solution. Region III: the antiphase and quasi-in-phase synchronized solutions. Region IV: the only in-phase synchronized solution. Region V: the in-phase and quasi-antiphase synchronized solutions. Regions VI and VIII: the in-phase and antiphase synchronized solutions. Region VII: the in-phase, quasi-antiphase, and antiphase synchronized solutions. Region IX: in addition to the antiphase synchronized solution, (i) the in-phase synchronized solution with alternating of the firing order of the two neurons exists. (ii) Figs. 3(b)–3(d)are demonstrated. (b) ϕ-β diagram for the linear stability as $G_{syn}=-0.4$ are illustrated. The solid and broken lines represent stable and unstable fixed points. β_2 and β_3 are saddle-node and inverse pitchfork bifurcation points, respectively. β_4 is a boundary point to split into type-I and -II TFPDs.

$$x_2^{--}(\Delta_1+\Delta_2+\Delta_3) = x_2^{--}(\Delta_1+\Delta_2)e^{-\gamma_0\Delta_3} + A_4(1-e^{-\gamma_0\Delta_3}) + B_2 s_1^{-}(\Delta_1+\Delta_2)(e^{-\beta\Delta_3} - e^{-\gamma_0\Delta_3}), \quad (49)$$

$$s_2^{-}(\Delta_1+\Delta_2+\Delta_3) = s_2^{-}(\Delta_1+\Delta_2)e^{-\beta\Delta_3}. \quad (50)$$

Here we have to consider the above described condition where neuron 2 arrives at the threshold (θ_1) earlier than neuron 1, $-\gamma_0(X_r-A_3)e^{-\gamma_0 T_3} + \beta B_2(e^{-\beta T_3} - e^{-\gamma_0 T_3}) < 0$. Based on such a condition, we then obtain

$$x_2^{--}(\Delta_1+\Delta_2+\Delta_3)=\theta_1. \tag{51}$$

The other state of the two neurons is also changed to $x_1^{-+}(\Delta_1+\Delta_2+\Delta_3)=x_1^{--}(\Delta_1+\Delta_2+\Delta_3)$, $x_2^{+-}(\Delta_1+\Delta_2+\Delta_3)X_u$, and $s_2^-(\Delta_1+\Delta_2+\Delta_3)\to s_2^+(\Delta_1+\Delta_2+\Delta_3)=1$.

Finally, we suppose that for $[\Delta_1+\Delta_2+\Delta_3, \Delta_1+\Delta_2+\Delta_3+\Delta_4]$, neurons 1 and 2 are in the inactive and active phases, respectively, and that at $t=\Delta_1+\Delta_2+\Delta_3+\Delta_4$ neuron 1 is at threshold θ_1 when it starts firing again. Then, making use of case (ii), the state of the two neurons is given by

$$\begin{aligned} x_1^{-+}(\Delta_1+\Delta_2+\Delta_3+\Delta_4) &= x_1^{-+}(\Delta_1+\Delta_2+\Delta_3)e^{-\gamma_0\Delta_4} \\ &\quad + A_3(1-e^{-\gamma_0\Delta_4})=\theta_1, \\ &\to x_1^{++}(\Delta_1+\Delta_2+\Delta_3+\Delta_4)=X_u, \end{aligned} \tag{52}$$

$$\begin{aligned} s_1^-(\Delta_1+\Delta_2+\Delta_3+\Delta_4) &= s_1^-(\Delta_1+\Delta_2+\Delta_3)e^{-\beta\Delta_4}, \\ &\to s_1^+(\Delta_1+\Delta_2+\Delta_3+\Delta_4)=1, \end{aligned} \tag{53}$$

$$\begin{aligned} x_2^{++}(\Delta_1+\Delta_2+\Delta_3+\Delta_4) &= x_2^{+-}(\Delta_1+\Delta_2+\Delta_3+\Delta_4) \\ &= x_2^{+-}(\Delta_1+\Delta_2+\Delta_3)e^{-\gamma_1\Delta_4}+A_2(1 \\ &\quad - e^{-\gamma_1\Delta_4})+B_1 s_1^-(\Delta_1+\Delta_2+\Delta_3) \\ &\quad \times(e^{-\beta\Delta_4}-e^{-\gamma_1\Delta_4}), \end{aligned} \tag{54}$$

$$s_2^+(\Delta_1+\Delta_2+\Delta_3+\Delta_4)=1. \tag{55}$$

Note that Eq. (54), which implicitly involves $x_2^{(n)}$, represents the state of neuron 2 when neuron 1 starts firing again. We arrive at the $(n+1)$th iterate of the return map for type-I TFPD and now obtain the explicit expression for the one-dimensional return map in terms of $x_2^{(n)}$,

$$x_2^{(n+1)}=x_2^{++}(\Delta_1+\Delta_2+\Delta_3+\Delta_4)=F^{(\mathrm{I})}(x_2^{(n)}). \tag{56}$$

It is more convenient to define the phase difference at the nth iterate between the two coupled neurons as

$$x_{dif}^{(n)}\equiv X_u-x_2^{(n)}, \quad (x_{dif}^{(n)}\geqslant 0). \tag{57}$$

We straightforwardly obtain a one-dimensional return map for the phase difference at the $(n+1)$th iterate,

$$\begin{aligned} x_{dif}^{(n+1)} &= F_1(x_{dif}^{(n)}), \\ &= X_u-F^{(\mathrm{I})}(X_u-x_{dif}^{(n)}), \quad (x_{dif}^{(n)}\geqslant 0). \end{aligned} \tag{58}$$

This return map is applicable for $(X_1+G_{syn})/\theta_2<\gamma_1<\infty$ as well as for a broad region of the parameter space of G_{syn} and β. Equation (58) is thus valid for (G_{syn},β) in the regions III–VIII of the G_{syn}-β plane [Fig. 2(a)]. This is because the condition in which neuron 2 reaches the threshold θ_1 earlier than neuron 1 is assumed to give Eq. (58) (see Appendix A). A return map for region IX of the G_{syn}-β plane of Fig. 2(a) is studied in Appendix B.

We now analyze the map $x_{dif}^{(n+1)}=F_1(x_{dif}^{(n)})$. Note that $x_{dif}=0$ is a fixed point solution of $x_{dif}^{(n+1)}=F_1(x_{dif}^{(n)})$ and gives rise to the in-phase synchronization of the two coupled neurons. The stability of this solution is examined by the linear stability analysis,

$$\begin{aligned} \frac{dF_1(0)}{dx_{dif}} &= \frac{\gamma_1(X_u-A_2)-G_{syn}e^{-\beta T_3}}{\gamma_1(X_u-A_1)} \\ &\quad \times \frac{\gamma_0(X_r-A_2)e^{-\gamma_0 T_3}-\beta B_2(e^{-\beta T_3}-e^{-\gamma_0 T_3})}{\gamma_0(\theta_1-A_3)}. \end{aligned} \tag{59}$$

This equation can also be obtained in a more intuitive manner as given in Appendix A. The stability condition is given by $0\leqslant dF_1/dx_{dif}|_{x_{dif}=0}<1$. For any (G_{syn},β) in regions IV–VIII of Fig. 2(a), we find that the above condition is satisfied and that the in-phase synchronized solution is stable. It is noted that for (G_{syn},β) in regions IV–VIII, the approach to the $x_{dif}=0$ solution is monotonic with time. It is furthermore noted that the quasi-antiphase and the quasi-in-phase ones would be also obtained by solving this map.

Next, we study the return map for the condition $-\gamma_0(X_r-A_3)e^{-\gamma_0 T_3}+\beta B_2(e^{-\beta T_3}-e^{-\gamma_0 T_3})>0$, which means that neuron 2 starts to fire after neuron 1 [i.e., $x_2^{--}(\Delta_1+\Delta_2+\Delta_3)<x_1^{--}(\Delta_1+\Delta_2+\Delta_3)$]. Here it is noted that the return map is different from Eq. (56), which can be satisfied with region IX of Fig. 2(a). The phase difference at the $(n+1)$th iterate is then defined as $y_{dif}^{(n+1)}=x_2^{(n+1)}-x_1^{(n+1)}(>0)$ at the time that neuron 2 reaches the threshold θ_1. Hence we have the new map

$$y_{dif}^{(n+1)}=F_2(x_{dif}^{(n)}). \tag{60}$$

Iterating this map once more, we have the map $x_{dif}^{(n)}\mapsto x_{dif}^{(n+2)}$,

$$x_{dif}^{(n+2)}=F_2(y_{dif}^{(n+1)})=F_2\circ F_2(x_{dif}^{(n)}). \tag{61}$$

Since $x_{dif}=0$ is a fixed point of the map, its stability condition is determined by

$$\begin{aligned} \left.\frac{dF_2\circ F_2(x_{dif})}{dx_{dif}}\right|_{x_{dif}=0} &= \left.\frac{dF_2[F_2(x_{dif})]}{dF_2(x_{dif})}\right|_{F_2(x_{dif})=0} \\ &\quad \times \left.\frac{dF_2(x_{dif})}{dx_{dif}}\right|_{x_{dif}=0} \\ &= \left[\frac{dF_2(0)}{dx_{dif}}\right]^2<1. \end{aligned} \tag{62}$$

We show that the stability condition Eq. (62) is satisfied with $dF_2(0)/dx_2<1$ for any (G_{syn},β) in region (ii) of IX. It is noted that the two neurons alternate their firing order and are attracted to the in phase synchronized solution. However, $dF_2(0)/dx_{dif}$ can increase beyond 1 and break down the stability condition of Eq. (62) for a certain interval of G_{syn}. Then, in region (i) of IX of Fig. 2(a), the in-phase synchronized solution becomes unstable. In addition, the stable (or unstable) fixed point solution for $x_{dif}=F_2\circ F_2(x_{dif})$ given by $x_{dif}\neq 0$ emerges, corresponding to the two neurons becoming synchronized with their constant (or irregular) phase difference and alternating (or, regularly and irregularly alternating) firing order as shown in Figs. 3(b)–3(d).

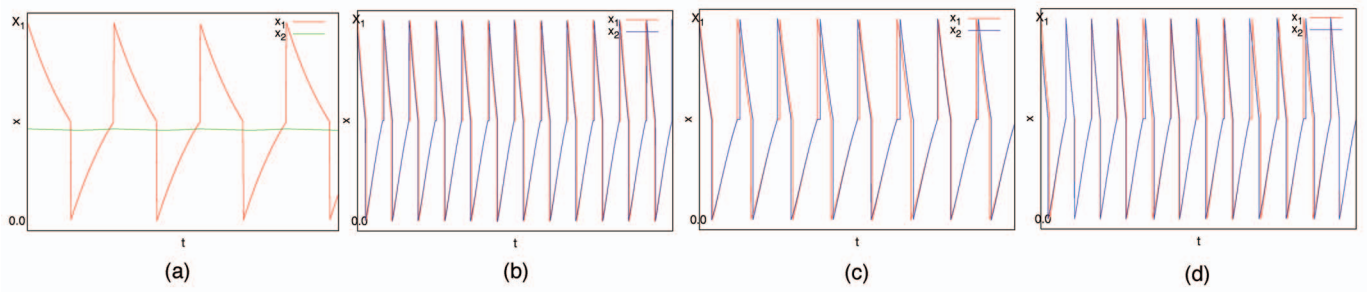

FIG. 3. (Color) Various types of synchronized solutions. (a) Death oscillators. (b) Two neurons become synchronized with a constant phase difference, alternating the firing order of the two neurons. (c) These neurons alternate their firing order, irregularly changing the phase difference. (d) In the two coupled neurons, the alternating, nonalternating of the firing order and their phase difference vary irregularly.

C. Antiphase synchronization

In order to investigate antiphase synchronization, we have to find a condition that will allow us to select type-II TFPD (as is shown in Table II) from various types of the TFPDs. The condition is found by investigating whether the well-known death oscillator [52,61] exists or not, that is, $T_5-T_5' \gtrless 0$. This is studied in Appendix A and corresponds to region I of Fig. 2(a). The death oscillator behaves as follows: One neuron continues to fire periodically while the other's membrane potential cannot arrive at the threshold θ_1 [Fig. 3(a)]. In this paper, we omit a return map for the death oscillator because this is checked by numerical simulation.

As $T_5-T_5'<0$, we can use the type-II TFPD to mainly analyze the occurrence of the antiphase synchronized solution, $\phi=0.5$. To investigate such synchronization behaviors, we consider nth iterate in the two neuron states as $x_1^{(n)} \equiv X_u$, $s_1^{(n)} \equiv 1$, $x_2^{(n)}$ and $s_2^{(n)}$, and then analyze a time evolution of Table II in the same manner as in Sec. III B. This results in the two-dimensional return map for studying the antiphase, which is represented by

$$\begin{pmatrix} x_2^{(n+1)} \\ s_2^{(n+1)} \end{pmatrix} = \mathbf{F}^{(\mathrm{II})}(x_2^{(n)}, s_2^{(n)}) \equiv \begin{pmatrix} F_1^{(\mathrm{II})}(x_2, s_2) \\ F_2^{(\mathrm{II})}(x_2, s_2) \end{pmatrix} = \begin{pmatrix} X_r e^{-\gamma_0 \Delta_4} + A_4(1-e^{-\gamma_0 \Delta_4}) + B_2 e^{-\beta(\Delta_2+\Delta_3)}(e^{-\beta\Delta_4} - e^{-\gamma_0\Delta_4}) \\ e^{-\beta\Delta_4} \end{pmatrix}, \tag{63}$$

where the values of $\Delta_4(\Delta_3, \Delta_2, \Delta_1, s_2)$, $\Delta_3(\Delta_2)$, $\Delta_2(\Delta_1, x_2)$, and $\Delta_1(s_2)$ are numerically obtained by the following equations:

$$\begin{aligned} &[\{X_r e^{-\gamma_0\Delta_2} + A_4(1-e^{-\gamma_0\Delta_2}) + B_2 s_2 e^{-\beta\Delta_1}(e^{-\beta\Delta_2} - e^{-\gamma_0\Delta_2})\} e^{-\gamma_0\Delta_3} \\ &\quad + A_3(1-e^{-\gamma_0\Delta_3})] e^{-\gamma_0\Delta_4} + A_4(1-e^{-\gamma_0\Delta_4}) \\ &\quad + B_2(e^{-\beta\Delta_4} - e^{-\gamma_0\Delta_4}) = \theta_1, \end{aligned} \tag{64}$$

$$X_u e^{-\gamma_1\Delta_3} + A_2(1-e^{-\gamma_1\Delta_3}) + B_1 e^{-\beta\Delta_2}(e^{-\beta\Delta_3} - e^{-\gamma_1\Delta_3}) = \theta_2, \tag{65}$$

$$\begin{aligned} &\{x_2 e^{-\gamma_0\Delta_1} + A_3(1-e^{-\gamma_0\Delta_1})\} e^{-\gamma_0\Delta_2} + A_4(1-e^{-\gamma_0\Delta_2}) \\ &\quad + B_2(e^{-\beta\Delta_2} - e^{-\gamma_0\Delta_2}) = \theta_1, \end{aligned} \tag{66}$$

$$X_u e^{-\gamma_1\Delta_1} + A_2(1-e^{-\gamma_1\Delta_1}) + B_1 s_2(e^{-\beta\Delta_1} - e^{-\gamma_1\Delta_1}) = \theta_2. \tag{67}$$

This return map is applicable in a wider region of (G_{syn}, β), namely, regions II–IX of Fig. 2(a), compared to the region in which the in-phase synchronized solution exists.

We investigate Eqs. (63)–(67) to obtain the equilibrium state $(x_2^{(\infty)}, s_2^{(\infty)})$. $(x_2^{(\infty)}, s_2^{(\infty)}) = \mathbf{F}^{(\mathrm{II})}(x_2^{(\infty)}, s_2^{(\infty)})$ by numerical calculations causes the quasi-antiphase and quasi-in-phase synchronized solutions to be acquired due to the parameters of our model. Its stability of the fixed point $(x_2^{(\infty)}, s_2^{(\infty)})$ is then determined by the roots of the characteristic equation

$$\left| \frac{\partial \mathbf{F}^{(\mathrm{II})}(x_2^{(\infty)}, s_2^{(\infty)})}{\partial(x_2, s_2)} - \lambda \mathbf{I} \right| = 0, \tag{68}$$

where $\mathbf{I}$ is a 2×2 unit matrix. The multiplier λ is the corresponding eigenvalue of the above Jacobian matrix and is given by

$$\lambda_\pm = \frac{p \pm \sqrt{p^2 - 4q}}{2},$$

$$p = \frac{\partial F_1^{(\mathrm{II})}}{\partial x_2} + \frac{\partial F_2^{(\mathrm{II})}}{\partial s_2},$$

$$q = \frac{\partial F_1^{(\mathrm{II})}}{\partial x_2}\frac{\partial F_2^{(\mathrm{II})}}{\partial s_2} - \frac{\partial F_1^{(\mathrm{II})}}{\partial s_2}\frac{\partial F_2^{(\mathrm{II})}}{\partial x_2}. \tag{69}$$

The numerical calculation of Eqs. (67)–(69) makes us deduce that the fixed point is linearly stable if $|\lambda_\pm|<1$ and unstable if $|\lambda_\pm|>1$ for at least one value of $\pm$, that is, λ_+

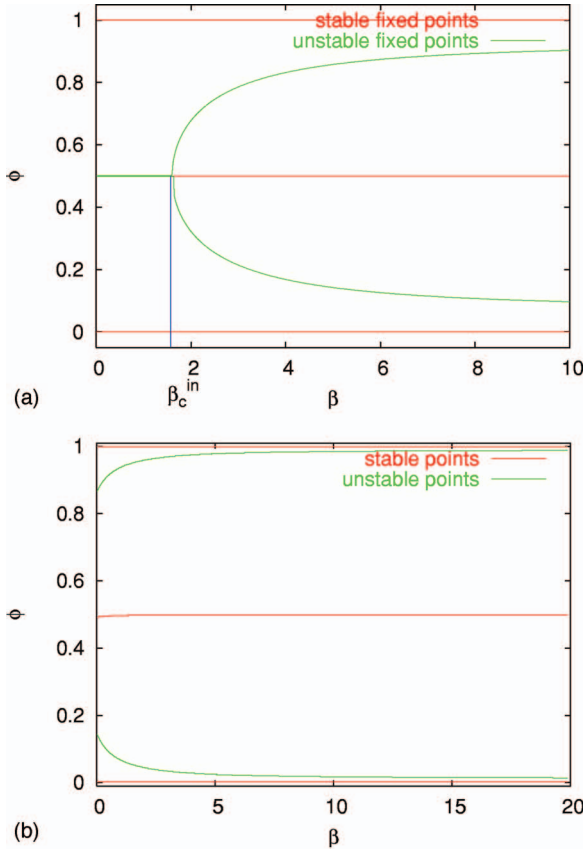

FIG. 4. (Color) β-ϕ bifurcation diagram. (a) and (b) are β-ϕ bifurcation diagrams for $\gamma_1=10$ and $\gamma_1=100$. Red and green lines, respectively, represent stable and unstable fixed points.

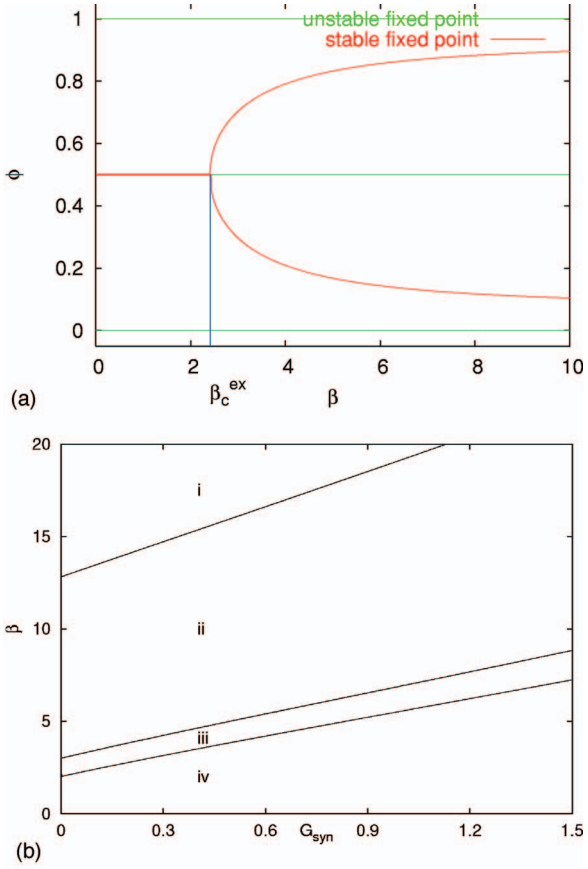

FIG. 5. (Color) Excitatory couplings for $\gamma_1=10$. (a) β-ϕ bifurcation diagram for $G_{syn}=0.1$. Red and green lines, respectively, represent stable and unstable fixed points. (b) G_{syn}-β phase diagram. Region i: type-I quasi-in-phase synchronized solution. Region ii: type-II quasi-in-phase synchronized solution. Region iii: type-II quasi-antiphase synchronized solution. Region iv: the antiphase synchronized solution. $\phi(x_2^{(\infty)},s_2^{(\infty)})=0.75$, which represents a boundary line between regions ii and iii, divides synchronized solution into the quasi-in-phase and quasi-antiphase ones.

>1. Hence a pitchfork bifurcation diagram in terms of type-II TFPD is locally obtained. For example, as we can see in Fig. 2(b), when β is small, the antiphase synchronized solution at $\phi(x_2^{(\infty)},s_2^{(\infty)})=0.5$ is unstable. At the critical value β_3, this solution becomes stable and two additional unstable solutions arise from the point $\phi=0.5$.

IV. ANALYTICAL AND NUMERICAL RESULTS OF THE COUPLED DIF MODELS

The whole return map is defined as $x_2^{(n)}$ in the regions $[X_r,\theta_1]$ and $[\theta_2,X_1]$ and for $s_2^{(n)}$ in $[0, 1]$. This can be obtained by incorporating other TFPDs as well as the TFPDs shown in Tables I and II. On the basis of such a return map, we calculate various synchronized states as $t\to\infty$ included in the transient dynamics. As a result, according to the differing duration of a firing (including the case of $\gamma_1\to\infty$), we demonstrate some parameter spaces of synaptic couplings (G_{syn}-β) [Figs. 2(a) and 5(b)] and plots of ϕ as a function of β [Figs. 2(b), 4(a), and 5(a)], resulting in the linear stability analysis for the system with the two coupled neurons. Now we set $\gamma_0=1$, $X_0=X_u=2$, $X_1=X_r=0$, and $\theta_1=\theta_2=1$. We show the results of the synchronization behavior of our system obtained theoretically and by numerical simulations.

A. Inhibitory synaptic coupling

We shall examine systematically the detailed behavior of the two DIF neuron models with inhibitory synaptic interactions, in order to understand the more theoretical analysis in Sec. III. For the case of $\gamma_1=1$, as dynamical behavior of the two neurons move toward a completely synchronous state, alternations in their firing order do not occur for (G_{syn},β) in regions IV–VIII of Fig. 2(a). In the weak strength regions of Fig. 2(a), saddle-node and inverse pitchfork bifurcations have been obtained by the linear stability analysis for type-I and -II TFPDs, respectively [see Fig. 2(b)]. Due to the coexistence of these bifurcations, a diversity of synchronization behaviors can be observed due to the differing values of G_{syn} and β. As $|G_{syn}|$ becomes larger, the phase state of the synchronized solution of the two neurons shifts to (G_{syn},β) in region IX. In addition to the antiphase synchronized solution, the two neurons become synchronized in the in-phase, temporarily alternating their firing orders (region ii in IX). For (G_{syn},β) of region i in IX, we can also see that the two neurons behave as shown in Figs. 3(b)–3(d), which have not been analytically and numerically investigated so far. When the minus quantity of G_{syn} becomes larger in region IX, the behaviors of the two neurons shift as follows: Fig. 3(b) →

Fig. 3(c) → Fig. 3(d). Finally, the continuing growth of $|G_{syn}|$ leads to a transition to region I exhibiting death oscillator.

When γ_1 is gradually increased, the saddle-node bifurcation disappears while the inverse pitchfork bifurcation begins to dominate in the ϕ-β diagram, as shown in Fig. 4(a). This is because type-II TFPD now becomes a more applicable diagram for our system than type-I TFPD. As β is small, the two neurons can simultaneously fire, independent of their neuronal states. For β larger, they are in the in-phase or antiphase synchronized states due to the initial conditions of our model. This is almost identical to the bifurcation diagram that has been already reported in [32,60]. This agreement enables us to expect that the width of an action potential would play an important role in inhibitory synchrony. For the weak coupling, tremendously complicated synchronous behavior such as regions III–VIII in Fig. 2(a) can be no longer monitored. There exists only the in-phase synchronized solution region and the region of co-exsistence of the in-phase and antiphase states For the strong coupling, the two-neuron behavior is almost kept under the actions as shown in Fig. 2(a).

As γ_1 becomes larger, an inverse pitchfork bifurcation point β_c^{in} of Fig. 4(a) decreases and then disappears for weak coupling. The β-ϕ diagram such as Fig. 4(b) (for $\gamma_1=100$) is then obtained. Finally, in the case taking the limit $\gamma_1 \to \infty$, we do not have to take type-I TFPD into account. This enables us to easily deduce that unstable quasi-in-phase synchronized solutions [which are shown by green lines in Fig. 4(a)] can undergo a transition to unstable in-phase synchronized solutions. We only need to perform the linear analysis of the firing time difference of neurons, which determines the boundary line between asynchronous and death oscillator states for (G_{syn}, β). Therefore the death oscillators are observed in a region of small β while the antiphase synchronized solution can also be obtained.

B. Excitatory synaptic couplings

We investigate synchronous behavior in two excitatory coupled DIF neurons having any values of γ_1. For weakly coupled DIF models, when γ_1 becomes progressively larger, one can see the pitchfork bifurcation by linear stability analysis [as shown in Fig. 5(a)]. The stable antiphase synchronized solution undergoes a transition to two stable quasi-antiphase and unstable antiphase ones as β becomes systematically larger. Similar to the case of inhibitory coupling, we have demonstrated such a pitchfork bifurcation result, which is in good agreement with [32,60].

For β small, as shown in Fig. 5(a), we have found it difficult for the two neurons to be in a synchronous state even though the coupling is strong. This is only because the pitchfork bifurcation point β_c^{ex} of Fig. 5(b) takes the larger value as G_{syn} becomes larger.

In the case of $\gamma_1 \gg 1$, the pitchfork bifurcation point of β_c^{ex} vanishes. Antiphase as well as in-phase synchronized solutions are unstable while the quasi-in-phase synchronized solution is stable for any β. This is the opposite stability result to Fig. 4(b). As a result, in addition to the differing degree of G_{syn}, the quasi-in-phase synchronized solution region such as region iv of Fig. 5(b) is transited to the whole β-G_{syn} diagram. Furthermore, taking the limit of $\gamma_1 \to \infty$, type-II TFPD can be solely applied so that the stable quasi-in-phase synchronized solutions turn into stable in-phase ones. Therefore for any (G_{syn}, β), we have demonstrated that the two neurons synchronously fire.

C. μ boundary of synchronous behavior

We shall confirm that a y-coupled system of Eqs. (18)–(20) is applicable and convenient for studying synchronization phenomena of neurons. For this, we employ a phase reduction analysis [48–52]. In the phase reduction analysis, we can reduce the weakly coupled oscillatory models to equations consisting of the phase degrees of freedom [Appendix C]. Using the obtained phase equations, we systematically give an explanation of the synchronization phenomena with a time scale parameter μ. The phase equations are obtained as follows:

$$\frac{d\phi(t)}{dt} = \epsilon[H_1(-\phi) - H_2(\phi)] \equiv G(\phi), \tag{70}$$

$$H_i(\phi) = \frac{1}{T}\int_0^T \{\mathbf{Z}_i(t)\}^T \cdot \mathbf{P}_i(t+\phi)dt \quad (i=1,2), \tag{71}$$

where $\phi=\Theta_1-\Theta_2$ denote the phase difference between the two neurons. It is noted that ϕ corresponds to the one in the return map analysis. G is expressed as an average interaction function of ϕ due to the different μ values. We assume that the coupling vectors P_i are $(0,-\mu s_i^-,0)^T$ and $(s_i^-,0,0)^T$. $\{\mathbf{Z}(t)\}^T$ is the so-called phase response curve, which can often be measured as a neuronal firing property. $G(\phi_0)=0$ so that the synchronized solution is a fixed point to our system. For $\epsilon>0$ (excitation), the solution is stable if $G'(\phi_0)<0$ while it is unstable if $G'(\phi_0)>0$. The stabilities for the inhibition system (that is, $\epsilon<0$) are opposite to those for the excitation system. Thus using such stabilities for $\beta>\beta_c^{\text{ex}}$ (or β_c^{in}), we can obtain a restraint condition to maintain synchronous behavior of Figs. 4(a) and 5(a).

For μ less than a critical value $\mu_c(\approx 0.35)$ [see Fig. 6(a)], the excitatory y-coupling system of the PL model have only stable quasi-in-phase and quasi-antiphase synchronized solutions, but also two unstable in-phase synchronized solutions and one unstable antiphase synchronized solutions. As μ is increased over μ_c, this system fails to have a stable quasi-in-phase synchronized solution. Only the unstable in-phase and stable antiphase synchronized solutions remain.

Synchronous states in an excitatory x-coupling system of the PL model should be contrasted with those in the y-coupling system, because the same set of solutions exists but all of their stabilities are reversed [Fig. 6(b)]. For μ small, stability analysis using the phase reduction method makes predictions about our previous investigation of [46]: For excitatory coupling with a large β, the two neurons become synchronized in the in- phase or antiphases depending on the initial conditions. When β is small, they become synchronized in-phase. For β large, the x-coupling system also has a critical value of μ_c (≈ 0.082), where two unstable syn-

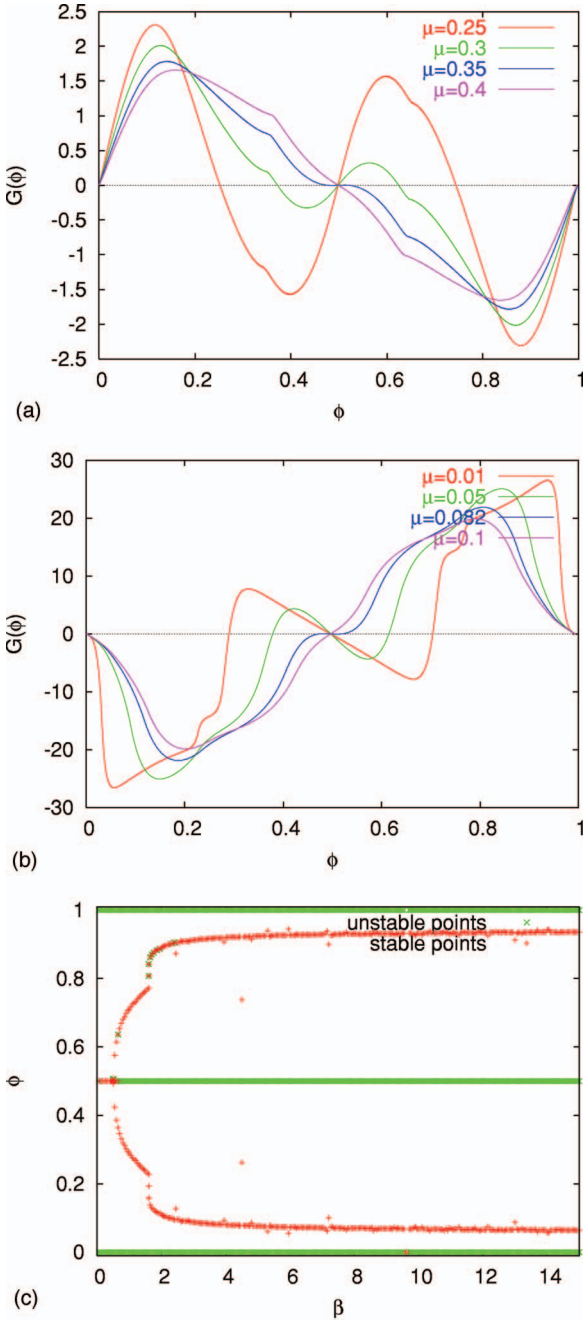

FIG. 6. (Color) Phase reduction analysis for FHN and PL model with a finite μ. (a) and (b), respectively, demonstrate G plotted as a function of the phase ϕ for y- and x-coupled system of the PL model with $\mu=0.01$, $p=2/3$, $q=0$, $m=n=2/3$, $\theta_1=-1$, and $\theta_2=1$. Four different μ values are shown. Stable or unstable equilibrium states correspond to 0 crossing with negative or positive slopes. (c) β-ϕ bifurcation diagram for a y-coupled system of FHN model [Eqs. (1) and (2)] with $\mu=0.01$. This agrees with numerical simulations for a y-coupled system of the PL model.

chronized solutions disappear, and only two stable in-phase and one unstable antiphase synchronized solutions remain. For the inhibitory y- or x-coupling systems, the stability results are opposite to those just described.

For the FHN model with a finite μ, similar results to the cases using the PL model are found. As an example, investigating the y-coupling system, we have depicted a pitchfork bifurcation diagram of Fig. 6(c). This is in good agreement with the results in this study using the DIF model. As μ is small, for small values of the synaptic relaxation decaying rate β, there are two plausible synchronized states exhibiting either $\phi=0$, 1 or $\phi=0.5$. Only $\phi=0.5$ is stable. With increasing β, corresponding to progressively faster decaying synapses, there is a pitchfork bifurcation at a critical value of β and two more equilibria are produced. The antiphase synchronized solution loses stability and continues as an unstable state. Two new stable solutions of the quasi-antiphase synchronized are generated. As μ is increased, the two quasi-antiphase synchronized states for large β disappear and then the antiphase synchronized solution is changed from unstable to stable.

V. DISCUSSION

In order to discuss whether the width of an action potential plays a role in generating synchronization phenomena, we summarize the return map analysis using our DIF models coupled via inhibitory or excitatory synapses.

For strong inhibitory coupling, irregular synchronous behavior can exist. Bressloff and Coombes [61] utilized two coupled IF models with the α function to reveal only the existence of death oscillators for strongly synaptic strength of the coupling. However, in our studies on the strongly coupled system, in addition to the death oscillators, irregular as well as antiphase synchronous behavior have been found. The remarkable point that we would like to stress in this paper is that the firing duration enables us to analytically obtain a diversity of such synchronous behavior. Here we notice that the synaptic coupling model in this paper is different from the α-function model. We would then have to investigate behavior in the DIF models with synaptic coupling exhibiting the α function.

On the other hand, for the weak coupling, reverse and normal pitchfork bifurcation sequences have been observed respectively as β in inhibition and excitation are changed [Figs. 4(a) and 5(a)]. In particular, an inhibitory synchrony occurs independent of β values. Such synchronization properties in the two coupled neurons were already shown [32]. It was suggested that the inhibition leads to a stable synchronous state unless the time scale for rising synaptic response is very short or the action potential is broad. However, our studies have shown that the inhibitory synchrony is not produced by slowly rising synaptic response. Moreover, the stable in-phase synchronized solutions remain even though the firing durations become extremely short, because type-I TFPD still works. Therefore the suggestion of [32] is not sufficient. We can say that our coupled system of the DIF model has a mathematically different property that the width of an action potential and synaptic responses that rise quickly but decay slowly make a pair of the weakly coupled neurons act as shown in Figs. 4(a) and 5(a).

Chow and Kopell suggested for the first time that spike shape and size play a large role in the generation of stable synchronous state in improved IF models with gap junctions [35]. They compared them to the cases for some biophysical

conductance-based models, but the case using the synaptic coupling was not explored. In the present study, we have investigated in detail how the width of an action potential γ_1 affects the synchronization properties in a pair of coupled oscillators, based on the relationship between the coupled IF model and the coupled PL model.

As for whether the broad action potential essentially affects the generation of inhibitory synchrony, there is still ample scope for discussion. However, we have found that the width of the action potential plays an important role in a phase transition of synchronous behavior, on the basis of the β-dependent bistable behavior of Figs. 4(a) and 5(a). Our studies have shown that coexistences of a variety of synchronous behavior result in the broad width.

We have applied a phase reduction method and numerical simulations to x- and y-coupling systems of the PL model with a finite μ for n and m values in Eq. (8). For n smaller, a slope of the right branch in the x nullcline becomes more gradual in the x-y phase plane. The time when the trajectory arrives at $x=\theta_2$ becomes faster. This means that the firing duration becomes shorter as n becomes smaller. On the other hand, for m larger, the left branch slope is sharper. The latency period during which the trajectory is on the inactive phase becomes longer. Thus when m is larger and n is smaller, the PL model with $\mu<\mu_c$ behaves more like the IF model.

Due to a large value of m and small one of n, we observe how weakly x- and y-coupled systems of the PL model behave. For the x-coupled system, with μ smaller than the critical value, the coexistence of in-phase and antiphase synchronized solutions is obtained for β larger, whereas only two in-phase synchronized solutions exist for a small β. We cannot observe a remarkable difference to our investigation of [46]. The y-coupled system also allows us to acquire the similar bifurcation diagrams such as Figs. 4(a) and 5(a).

Therefore we have found that as $\mu<\mu_c$ is taken into account, synchronous behavior in the x-coupled system of the PL model are not dependent of the width of an action potential, whereas the y-coupled system allows us to give an analytical explanation of how the width of an action potential affects synchronization phenomena, similar to the case in the limit of $\mu\to 0$.

Furthermore, we compare systematic synchronous behavior in x- or y-coupled PL model to the ones in coupled HH model of type-I or type-II. In [46], the x-coupled PL model with excitatory or inhibitory coupling behaves according to stabilities of their synchronous behavior, which can be opposite to the results of Figs. 5(a) or 4(b). We already showed that such a behavior in the x-coupled PL model is consistent to the result for using the type II HH model, independent of the value of μ. Employing the phase reduction method, we have shown that the pair system of the y-coupled PL model under a certain region of μ demonstrates like behavior of the type I HH model [62].

VI. CONCLUSION

In conclusion, our coupled system in the present work is an analytically solvable model having a firing duration and mutually coupled via synapses that rise quickly but decay slowly. It has some unique mathematical properties as well. One of them can make synchronous behavior in weakly coupled oscillators, which have been reported before. We have also demonstrated how the width of an action potential of neuron models influences a scheme of synchronized oscillations. In particular, we have given the following condition to increase the probability of synchrony in our model, independent of any β values: $\gamma_1 \gtrsim 100$ make inhibitorily coupled neurons achieve complete synchronization, although they have the coexistence of an antiphase synchronized solution. The condition of γ_1 has also enabled excitatorily coupled neurons to fire more and more in synchrony. However, it should be noted that complete synchronization has been observed.

We have clarified that our obtained results in an exactly solvable approach taking the limit $\mu\to 0$ have agreed precisely with those of numerical simulations and the phase reduction analysis for the PL or FHN models with small $\mu<\mu_c$. This has given us good support for the use of the DIF model [Eqs. (18)–(20)] to investigate synchronization phenomena of two coupled neurons.

Clarifying some aspects of the relationship between synaptically coupled systems of a pair of the IF and the PL models, we have shown an obvious difference in effect between insertions of coupling terms in the x or y dynamics, on the synchronization phenomena in two coupled neurons, and have interpreted the dynamical meaning of the y-coupled system as unifying theoretically tractable models. In particular, the x-coupled and y-coupled PL models are respectively capable of demonstrating the synchronous behavior of the coupled type I and type II HH model.

ACKNOWLEDGMENTS

The author would like to thank H. Daido, Y. Tsuchiya, Y. Miyake, D. Takashita, S. Bahar, and P. Wolfrum for some helpful discussions during the completion of this work. This work was supported by the 21st Century COE Program at Tokyo Tech "Nanometer-Scale Quantum Physics" by the Ministry of Education, Culture, Sports, Science and Technology. This work was financially supported by Hertie Foundation and 2005/2006 DAAD Research Grants for Doctoral Candidates and Young Academics and Scientists.

APPENDIX A: LINEAR ANALYSIS OF THE FIRING TIME DIFFERENCE OF NEURONS NEAR θ_1

We investigate each condition for the occurrence of the following cases: (i) Neuron 2 arrives at the threshold (θ_1) earlier than neuron 1. (ii) The existence of death oscillator.

To study the condition of the first case, we analyze the state of neuron 1 (or neuron 2) near the firing threshold, supposing Δ_1 and Δ_2 to be infinitesimally small, $\Delta_1=T_1+\delta s_1$ and $\Delta_2=0+\delta s_2$, we set $\Delta_3=T_3+\delta s_3$ (or $\Delta_3=T_3+\delta s_3'$). Here, it takes T_1 for the two neurons to drop down simultaneously to the inactive phase after they have fired. T_3 shows the duration in which they simultaneously enter again into the active phase since they finished firing. Considering the

moment when neuron 1 arrives at $x_1=\theta_1$ again, we have

$$X_r e^{-\gamma_0(T_3+\delta s_3)} + A_4\{1-e^{-\gamma_0(T_3+\delta s_3)}\} + B_2 e^{-\beta(0+\delta s_2)}\{e^{-\beta(T_3+\delta s_3)} - e^{-\gamma_0(T_3+\delta s_3)}\} = \theta_1. \tag{A1}$$

Up to the first order in δs_2 and δs_3, we obtain δs_3:

$$\delta s_3 = \frac{\beta B_2(e^{-\beta T_3}-e^{-\gamma_0 T_3})}{-\gamma_0(X_r-A_4)e^{-\gamma_0 T_3} + B_2(-\beta e^{-\beta T_3}+\gamma_0 e^{-\gamma_0 T_3})}\delta s_2, \tag{A2}$$

where T_3 is satisfied with the following equation:

$$X_r e^{-\gamma_0 T_3} + A_4(1-e^{-\gamma_0 T_3}) + B_2(e^{-\beta T_3}-e^{-\gamma_0 T_3}) = \theta_1. \tag{A3}$$

Similarly, suppose that neuron 2 starts to shift up to the active phase. Using the aforementioned analysis, we obtain $\delta s_3'$:

$$\delta s_3' = \frac{\gamma_0(X_r-A_3)e^{-\gamma_0 T_3}}{-\gamma_0(X_r-A_4)e^{-\gamma_0 T_3} + B_2(-\beta e^{-\beta T_3}+\gamma_0 e^{-\gamma_0 T_3})}\delta s_2. \tag{A4}$$

By $\delta s_3'-\delta s_3$, we can determine which of neurons 1 or 2 arrives earlier at the firing threshold. As an example, a solid boundary line of regions VI (or VIII) and IX of Fig. 2(a), which corresponds to $\delta s_3'-\delta s_3=0$, gives us the resulting equation:

$$-\gamma_0(X_r-A_3)e^{-\gamma_0 T_3} + \beta B_2(e^{-\beta T_3}-e^{-\gamma_0 T_3}) = 0. \tag{A5}$$

In Fig. 2(a), regions III–VIII indicate that neuron 2 reaches the threshold (θ_1) earlier than neuron 1 ($\delta s_3'-\delta s_3>0$), whereas region IX demonstrates that neuron 1 arrives at the threshold earlier than neuron 2 ($\delta s_3'-\delta s_3<0$).

Next, we examine the condition in which one neuron continues firing while the other is at rest. Assuming $\delta s_3'-\delta s_3<0$ of the condition for the occurrence of the first case, the subsequent temporal firing pattern diagram (TFPD) illustrates that neuron 2 keeps being in an inactive phase before the two neurons are not firing. We then suppose $\Delta_4=T_4+\delta s_4$ to be set up with $\Delta_5=T_5+\delta s_5$ (or $\Delta_5=T_5'+\delta s_5'$) if neuron 1 (or 2) arrives at θ_1 earlier than neuron 2 (or 1) at $t\Delta_1+\Delta_2+\Delta_3+\Delta_4+\Delta_5$. Using calculations for the zero order of δs_4, δs_5, and $\delta s_5'$, T_5 and T_5' are given as solutions of the following equations:

$$X_r e^{-\gamma_0 T_5} + A_4(1-e^{-\gamma_0 T_5}) + B_2 e^{-\beta(T_3+T_4)}(e^{-\beta T_5}-e^{-\gamma_0 T_5}) = \theta_1, \tag{A6}$$

$$\{X_r e^{-\gamma_0 T_3} + A_4(1-e^{-\gamma_0 T_3}) + B_2(e^{-\beta T_3}-e^{-\gamma_0 T_3})\}e^{-\gamma_0 T_4} + A_3(1-e^{-\gamma_0 T_4})]e^{-\gamma_0 T_5'} + A_4(1-e^{-\gamma_0 T_5'}) + B_2(e^{-\beta T_5'}-e^{-\gamma_0 T_5'}) = \theta_1, \tag{A7}$$

where T_3 and T_4 are satisfied by Eq. (A5) and $X_u e^{-\gamma_1 T_4} + A_2(1-e^{-\gamma_1 T_4}) + B_1 e^{-\beta T_3}(e^{-\beta T_4}-e^{-\gamma_1 T_4}) = \theta_2$. From a difference of T_5' and T_5, we then get the condition where the death oscillator occurs. The solid boundary line of regions I and II in Fig. 2(a) is given by

$$T_5'-T_5=0. \tag{A8}$$

APPENDIX B: RETURN MAPS FOR IN PHASE SYNCHRONIZATION

According to the inequality $\delta s_3'-\delta s_3 \gtrless 0$, we have two cases of TFPDs based on which the corresponding return map can be constructed. The two cases are displayed as III–VIII, and IX in the phase diagram of Fig. 2(a).

Regions III–VIII can also be explained as $\delta s_3'-\delta s_3>0$. Using Eqs. (18)–(20), we have the return map for a phase difference x_{dif}

$$F_1(x_{dif}) = (X_u-A_2)(1-e^{-\gamma_1\Delta_4}) - B_1 e^{-\beta\Delta_3}(e^{-\beta\Delta_4}-e^{-\gamma_1\Delta_4}), \tag{B1}$$

where $\Delta_4(\Delta_3,\Delta_2)$ and $\Delta_3(\Delta_2)$ are given by

$$\{X_r e^{-\gamma_0\Delta_3} + A_4(1-e^{-\gamma_0\Delta_3}) + B_2 e^{-\beta\Delta_2}(e^{-\beta\Delta_3}-e^{-\gamma_0\Delta_3})\}e^{-\gamma_0\Delta_4} + A_3(1-e^{-\gamma_0\Delta_4}) = \theta_1, \tag{B2}$$

$$\{X_r e^{-\gamma_0\Delta_2} + A_3(1-e^{-\gamma_0\Delta_2})\}e^{-\gamma_0\Delta_3} + A_4(1-e^{-\gamma_0\Delta_3}) + B_2(e^{-\beta\Delta_3}-e^{-\gamma_0\Delta_3}) = \theta_1. \tag{B3}$$

Region IX, $\delta s_3'-\delta s_3<0$. We have

$$F_2(x_{dif}) = (A_2-X_u)(1-e^{-\gamma_1\Delta_4}) + B_1 e^{-\beta(\Delta_3+\Delta_2)}(e^{-\beta\Delta_4}-e^{-\gamma_1\Delta_4}), \tag{B4}$$

where $\Delta_4(\Delta_3,\Delta_2)$ and $\Delta_3(\Delta_2)$, respectively, satisfy the following equations:

$$[\{X_r e^{-\gamma_0\Delta_2} + A_3(1-e^{-\gamma_0\Delta_2})\}e^{-\gamma_0\Delta_3} + A_2(1-e^{-\gamma_0\Delta_3}) + B_2(e^{-\beta\Delta_3}-e^{-\gamma_0\Delta_3})]e^{-\gamma_0\Delta_4} + A_3(1-e^{-\gamma_0\Delta_4}) = \theta_1, \tag{B5}$$

$$X_r e^{-\gamma_0\Delta_3} + A_4(1-e^{-\gamma_0\Delta_3}) + B_2 e^{-\beta\Delta_2}(e^{-\beta\Delta_3}-e^{-\gamma_0\Delta_3}) = \theta_1. \tag{B6}$$

Moreover, $\Delta_2(\Delta_1)$ and $\Delta_1(x_{dif})$ comply with the following equations:

$$\{X_u e^{-\gamma_1\Delta_1} + A_1(1-e^{-\gamma_1\Delta_1})\}e^{-\gamma_1\Delta_2} + A_2(1-e^{-\gamma_1\Delta_2}) + B_1(e^{-\beta\Delta_2}-e^{-\gamma_1\Delta_2}) = \theta_2, \tag{B7}$$

$$(X_u-x_{dif})e^{-\gamma_1\Delta_1} + A_1(1-e^{-\gamma_1\Delta_1}) = \theta_2. \tag{B8}$$

To conduct the linear stability analysis of $x_{dif}^{(n+1)}=F_1(x_{dif}^{(n)})$, we calculate the derivative of $F_1(x_{dif}^{(n)})$ at $x_{dif}=0$,

$$\left.\frac{dF_1}{dx_{dif}}\right|_{x_{dif}=0} = \left\{\left[\frac{\partial F_1}{\partial\Delta_4}\left(\frac{\partial\Delta_4}{\partial\Delta_3}\frac{\partial\Delta_3}{\partial\Delta_2}+\frac{\partial\Delta_4}{\partial\Delta_2}\right) + \frac{\partial F_1}{\partial\Delta_3}\frac{\partial\Delta_3}{\partial\Delta_2}\right]\frac{\partial\Delta_2}{\partial\Delta_1}\frac{d\Delta_1}{dx_{dif}}\right\}_{\Delta_1=T_1,\Delta_2=0,\Delta_3=T_3,\Delta_4=0}. \tag{B9}$$

Using Eqs. (B8) and (B3), T_1 and T_3 satisfy

$$X_u e^{-\gamma_1 T_1} + A_1(1 - e^{-\gamma_1 T_1}) = \theta_2, \tag{B10}$$

$$X_r e^{-\gamma_0 T_3} + A_4(1 - e^{-\gamma_0 T_3}) + B_2(e^{-\beta T_3} - e^{-\gamma_0 T_3}) = \theta_1. \tag{B11}$$

It then follows that Eq. (59) is acquired. Furthermore, the phase boundary between the phases of VIII and IX, which is defined by $\delta s_3' - \delta s_3 = 0$ with infinitesimally small Δ_2 and Δ_4, is given by

$$\gamma_0(X_r - A_3)e^{-\gamma_0 T_3} - \beta B_2(e^{-\beta T_3} - e^{-\gamma_0 T_3}) = 0. \tag{B12}$$

APPENDIX C: PHASE REDUCTION METHOD

The phase reduction analysis is briefly reviewed. The detailed analysis is referred to [62,63]. Supposing a pair of identical mutually x- (or y-) coupled PL or FHN neuron models when the synaptic coupling is weak ($\epsilon \ll 1$), we apply this method to the neuron models:

$$\frac{d\mathbf{X}_i}{dt} = F(\mathbf{X}_i) + \epsilon P_i[\mathbf{X}_{\bar{i}}(t)], \tag{C1}$$

where $F(\mathbf{X}_i)$ is a vector field as given by Eqs. (1) and (2) of the FHN model or Eqs. (4)–(8) of the PL model. Here we give two following definitions: (i) $\mathbf{X}_0(t)$ is the unique phase asymptotically stable T-periodic function to $d\mathbf{X}/dt = F(\mathbf{X})$. (ii) $\mathbf{Z}(t)$ is the unique solution to

$$\frac{d\mathbf{Z}(t)}{dt} = -[D_X F(\mathbf{X}_0(t))]^T \mathbf{Z}(t), \tag{C2}$$

where the normalization condition $\{\mathbf{Z}(t)\}^T \cdot [d\mathbf{X}_0(t)/dt] = 1$ is satisfied for every t. $\mathbf{Z}(t)$ is not only the phase response curve, but also the adjoint solution to the linearization around the limit cycle.

For ϵ small, we can apply averaging to the coupled system, to find

$$\frac{d\Theta_1}{dt} = 1 + \epsilon H_1(\Theta_1 - \Theta_2), \tag{C3}$$

$$\frac{d\Theta_2}{dt} = 1 + \epsilon H_2(\Theta_2 - \Theta_1), \tag{C4}$$

$$H_i(\phi) = \frac{1}{T}\int_0^T \{\mathbf{Z}_i(t)\}^T \cdot \tilde{\mathbf{P}}_i(t + \phi)dt, \tag{C5}$$

where $\tilde{\mathbf{P}}_i(t) = \mathbf{P}_i[\mathbf{X}_{\bar{i}}(t)]$. Let $\phi = \Theta_1 - \Theta_2$ denote the phase difference between the two neurons. We thus obtain the following phase equation:

$$\frac{d\phi}{dt} = \epsilon[H_2(-\phi) - H_1(\phi)]. \tag{C6}$$

[1] E. Basar, *Brain Function and Oscillations I: Brain Oscillations. Principles and Approaches* (Springer-Verlag, Berlin, 1998).
[2] H. Haken, *Brain Dynamics—Synchronization and Activity Patterns in Pulse-Coupled Neural Nets with Delays and Noise* (Springer-Verlag, Berlin, 2002).
[3] B. Lindner, J. Garcia-Ojalvo, A. Neiman, and L. Schimansky-Geier, Phys. Rep. **392**, 321 (2004).
[4] Q. Y. Wang, Q. S. Lu, G. R. Chen, and D. H. Guo, Phys. Lett. A **356**, 17 (2006).
[5] C. M. Gray, P. König, A. K. Engel, and W. Singer, Nature (London) **338**, 334 (1989).
[6] R. Eckhorn, A. Frien, R. Bauer, T. Woelbern, and H. Kehr, NeuroReport **4**, 243 (1993).
[7] A. K. Kreiter and W. Singer, J. Neurosci. **16**, 2381 (1996).
[8] D. Golomb and J. Rinzel, Physica D **72**, 259 (1994).
[9] N. Brunel, J. Physiol. (London) **94**, 445 (2000).
[10] G. Mongillo and D. J. Amit, J. Comput. Neurosci. **11**, 249 (2001).
[11] W. Gerstner and W. M. Kistler, *Spiking Neuron Models. Single Neurons, Populations, Plasticity* (Cambridge University Press, Cambridge, England, 2002).
[12] A. Karantonis, Y. Miyakita, and S. Nakabayashi, Phys. Rev. E **65**, 046213 (2002).
[13] Y. Miyakita, A. Karantonis, and S. Nakabayashi, Chem. Phys. Lett. **362**, 461 (2002).
[14] N. Brunel, V. Hakim, and M. J. E. Richardson, Phys. Rev. E **67**, 051916 (2003).
[15] D. T. W. Chik and Z. D. Wang, Phys. Rev. E **68**, 031907 (2003).
[16] A. Di Garbo, M. Barbi, and S. Chillemi, BioSystems **67**, 45 (2002).
[17] M. Nomura, T. Fukai, and T. Aoyagi, Neural Comput. **15**, 2179 (2003).
[18] A. L. Hodgkin and A. F. Huxley, J. Physiol. (London) **117**, 500 (1952).
[19] J. A. Connor, D. Walter, and R. McKown, Biophys. J. **18**, 81 (1977).
[20] C. Morris and H. Lecar, Biophys. J. **35**, 193 (1981).
[21] T. R. Chay and J. Keizer, Biophys. J. **42**, 181 (1983).
[22] L. Lapicque, J. Physiol. Pathol. Gen. **9**, 620 (1907).
[23] R. FitzHugh, *Biological Engineering*, edited by H. P. Schwan (McGraw-Hill, New York, 1969), p. 1.
[24] T. Yanagita, T. Ichinomiya, and Y. Oyama, Phys. Rev. E **72**, 056218 (2005).
[25] H. P. McKean, Adv. Math. **4**, 209 (1970).
[26] D. Hansel, G. Mato, and C. Meunier, Neural Comput. **7**, 307 (1995).
[27] G. B. Ermentrout, Neural Comput. **8**, 979 (1996).
[28] R. G. Kavasseri, *Proceedings of the Hawaii International Conference on Sciences Honolulu*, 2004.
[29] J. Keener and J. Sneyd, *Mathematical Physiology* (Springer-Verlag, New York, 1998).
[30] A. Longtin, Chaos **5**, 209 (1995).
[31] R. E. Mirollo and S. H. Strogatz, SIAM J. Appl. Math. **50**, 1645 (1990).

[32] C. Van Vreeswijk, L. F. Abbott, and G. B. Ermentrout, J. Comput. Neurosci. **1**, 1313 (1994).
[33] C. C. Chen, Phys. Rev. E **49**, 2668 (1994).
[34] V. Kirk and E. Stone, Phys. Lett. A **232**, 70 (1997).
[35] C. C. Chow and N. Kopell, Neural Comput. **12**, 1643 (2000).
[36] Y. D. Sato, Phys. Lett. A **319**, 486 (2003).
[37] A. Tonnelier and W. Gerstner, Phys. Rev. E **67**, 021908 (2003).
[38] D. Somers and N. Kopell, Biol. Cybern. **68**, 393 (1993).
[39] S. Coombes, Physica D **160**, 173 (2001).
[40] M. Denman-Johnson and S. Coombes, Phys. Rev. E **67**, 051903 (2003).
[41] D. Terman and D. L. Wang, Physica D **81**, 148 (1995).
[42] X. J. Wang and G. Buzsáki, J. Neurosci. **16**, 6402 (1996).
[43] H. R. Wilson, *Spikes, Decisions, and Actions—The Dynamical Foundations of Neuroscience* (Oxford University Press, New York, 1999).
[44] G. Renversez, Physica D **114**, 114 (1998).
[45] A. Bose, N. Kopell, and D. Terman, Physica D **140**, 69 (2000).
[46] Y. D. Sato and M. Shiino, Phys. Rev. E **66**, 041903 (2002).
[47] S. R. Campbell, D. L. Wang, and C. Jayaprakash, IEEE Trans. Neural Netw. **15**, 1027 (2004).
[48] J. C. Neu, SIAM J. Appl. Math. **37**, 307 (1979).
[49] Y. Kuramoto, *Chemical Oscillations, Waves, and Turbulence* (Springer-Verlag, Berlin, 1984).
[50] F. C. Hoppensteadt and E. M. Izhikevich, *Weakly Connected Neural Networks* (Springer-Verlag, Berlin, 1997).
[51] E. M. Izhikevich, SIAM J. Appl. Math. **60**, 1789 (2000).
[52] G. B. Ermentrout and N. Kopell, SIAM J. Appl. Math. **50**, 125 (1990).
[53] P. Frankel and T. Kiemel, SIAM J. Appl. Math. **53**, 1436 (1993).
[54] P. R. Adams, S. W. Jones, P. Pennefather, D. A. Brown, C. Koch, and C. Lancaster, J. Exp. Biol. **124**, 259 (1986).
[55] D. Kleinfeld, F. Raccuia-Behling, and H. J. Chiel, Biophys. J. **57**, 697 (1990).
[56] N. I. Syed, G. M. Bulloch, and K. Lukowiak, Science **250**, 282 (1990).
[57] L. F. Abbott and T. B. Kepler, in *Statistical Mechanics of Neural Networks*, Lecture Notes in Physics Vol. 368, edited by L. Garrido (Springer-Verlag, Berlin, 1990), p. 5.
[58] D. T. W. Chik, S. Coombes, and Z. D. Wang, Phys. Rev. E **70**, 011908 (2004).
[59] G. B. Ermentrout and C. C. Chow, Physiol. Behav. **77**, 629 (2002).
[60] C. van Vreeswijk, Phys. Rev. E **54**, 5522 (1996).
[61] P. C. Bressloff and S. Coombes, Phys. Rev. Lett. **81**, 2168 (1998).
[62] Y. D. Sato, Ph.D. thesis, Tokyo Institute of Technology, 2005 (unpublished).
[63] B. Ermentrout, Neural Comput. **15**, 2483 (2003).